**WOOD RESEARCH**
**64 (6): 2019**
**1065-1076**

# VENEER WARPAGE DEFORMATION MEASUREMENT BASED ON 3D LASER SCANNING TECHNOLOGY

Zhu Yuehua, Pan Biao, Zhang Yaoli
Nanjing Forestry University
Nanjing, China

(Received January 2019)

## ABSTRACT

In this paper, the warpage of the *Taxodium* hybrid 'zhongshanshan' veneer was measured by 3D laser scanning technology. The results showed that, the deformation of this veneer was mainly due to the warpage phenomenon along the cross striation of the wood. Air-drying shrinkage clearly enlarged the length in the direction of cross striation compared to the direction of parallel grain. The air-dried veneer would incline 7-12° along the direction of the parallel axis. When peeling the wood of the *Taxodium* hybrid 'zhong shan shan', the diameter decreased, and the warpage degree of veneer increased. The average veneer warpage degree of sapwood was 21.18%, the intermediate wood was 28.20%, and the heartwood near piths was 40.88%. High resolution 3D laser scanning technology accurately, intuitively, and rapidly obtained the deformation of the veneer.

KEYWORDS: Veneer, *Taxodium* hybrid 'zhongshanshan', 3D laser scanning technology, warpage deformation.

## INTRODUCTION

The *Taxodium* hybrid 'zhongshanshan' is an excellent tree species that is cultivated by artificial hybridization in the Institute of Botany, Chinese Academy of Sciences in Jiangsu Province. Based on its characteristics of salt-alkali tolerance, rapid growth, and good drying shape of *Taxodium mucronatum* Tenore, a *Taxodium* interspecific hybridization experiment and rapid-growing salt-alkali tolerance type selection were conducted. Many of the varieties were approved by the National Forestry Administration Forest Variety Examination Committee and Jiangsu Provincial Forest Variety Examination Committee, and entered the national and Jiangsu Provincial Forest Variety Examination List (Hua et al. 2017, Shi et al. 2016).

Studies on the wood properties of *Taxodium* hybrid 'zhongshanshan' indicated that the average density of wood was 0.3474 - 0.3620 $g \cdot cm^{-3}$, the radial total shrinkage rate was 1.98%, the tangential total shrinkage rate was 7.10%, the volume total shrinkage rate was 14.47%, the average

compressive strength along wood parallel grain was 25.85 MPa, the average bending strength was 41.98 MPa, the average modulus of flexural elasticity was 1741.78 MPa, and the average impact toughness was 129.61 $kJ \cdot m^{-2}$. The average hardness values of the end, chord, and diameter of the wood were 4377 N, 3897 N, and 3341 N, respectively (Yu et al. 2007, Zhao et al. 2007). During the rotary cutting process of *Taxodium* hybrid 'zhongshanshan' veneer, the deformation of the veneer was large, which is not conducive to the development and utilization of wood of the *Taxodium* hybrid 'zhongshanshan'.

Recently, the research on veneer quality has focused on the rapid and accurate measurement of the veneer surface roughness and the description of surface texture, as well as the measurement of veneer lathe checks and the effect of these veneer lathe checks on the veneer performance (Wang et al. 2001, Olenska et al. 2014). The evaluation on warpage is an important factor for the judgment of the veneer quality, which was often directly measured via straight ruler, by measuring the maximum deviation height between the veneer surface and the plane compared to the width of the veneer (Kong et al. 2018). In the practical measurement, the four angles of veneer after deformation were not on the same plane, which made the measurement difficult and the obtained data inaccurate.

3D laser scanning technology is a new technology for automation and visualization, which integrates optics, mechanics, electricity, and computer technology. It is mainly used to scan the spatial shape of an object to obtain the spatial coordinates of the object surface. The solid information is then converted to a digital signal that can be directly processed by computers and provides a very convenient and fast means for physical digitization (Krajewski et al. 2018).

3D laser scanning technology has been used for deformation measurement in many fields, such as the deformation measurement of structures (Rafa et al. 2018), the pavement deformation monitoring (Gui et al. 2018), and the tensile strain measurement of wood-plastic composites (Mbarek et al. 2011). These studies showed that 3D laser scanning technology could quickly and accurately measure micro-deformation at high resolution. It could also record 3D data and analyze deformation.

In wood research, the laser scanning of a wood cross section generated clear and contrasting images, which could quantitatively calculate the failure percentage of wood failure samples, evaluate the wood failure degree, and identify various surface anomalies. It achieved good accuracy and repeatability (Scott et al. 2005). Using a combination of 3D laser emitter and high-performance camera to scan the transverse section of a veneer (Bartosz et al. 2010), the scanned data can be converted into binary images by an algorithm to measure the lathe checks of veneers. Experimental results indicated this as an effective, high-yield, and direct method for measuring the lathe checks of veneers on production lines. Its measuring speed could be adjusted up to 7 $m \cdot min^{-1}$. It could be used to measure a board with a maximum thickness of 4 mm, and its resolution reached 0.01 mm.

However, the above test method has high requirements on the deformation of the specimen itself. Excessive deformation of the specimen would greatly impact the focus of the camera, resulting in a decline of data accuracy. By using non-contact high-resolution 3D laser scanning technology, the wood preserved in wet environment could be scanned and analyzed. The data of archaeological timber could be stored quickly and effectively without being influenced by environmental changes. The 3D laser scanning technology enables the recording and identification of archaeological timber in 3D, and the archaeological timber could be measured and modelled in the digital environment (Lobb et al. 2010). In this study, high resolution 3D laser scanning technology was used to study the deformation of *Taxodium* hybrid 'zhongshanshan' veneer, to provide a scientific basis for the measurement of warpage deformation of veneer.

## MATERIAL AND METHODS

### Experimental materials

The *Taxodium* hybrid 'zhongshanshan' veneer was taken from garden seedlings of the experimental demonstration base of the Institute of Botany, Chinese Academy of Sciences in Liuhe District, Nanjing City in Jiangsu Province. The average tree age was 15 years, the average tree height was 20.1 m, and the average diameter at breast height was 30.3 cm. The log of *Taxodium* hybrid 'zhongshanshan' was cut into 1.3 m, and the moisture content of the green wood was 109.81%.

### Experimental instruments and equipment

A BXQ (J) 1813 spindleless rotary cutting machine was obtained from Shandong Dongwei Woodworking Machinery Co., Ltd. A SZX7 stereo microscope and DP70 micro digital camera were obtained from Olympus in Japan. Handy SCAN 700 3D laser scanner was obtained from Creaform Company in Canada.

### Preparation of specimens

The logs of *Taxodium* hybrid 'zhongshanshan' were cut into veneer, and the veneer thickness was set to 2.00 mm. Specific materials during the rotary cutting process were selected, including the sapwood section (diameter 280-300 mm, marked S), the intermediate wood section (diameter 130-150 mm, marked S-H), and the section of the heartwood near pith (diameter 50-80 mm, marked H). Other veneers (1270 × 870 mm) were cut into several pieces (400 × 400 mm), and these pieces were then dried naturally to the moisture content 10-12%.

### Measurement of veneer back cracks

Several specimens with a length and width of 50 × 50 mm were taken from both ends of the three types of veneers in the direction of alignment, and then, these specimens were uniformly painted with pigments on their backs. After the pigments had completely dried, they were cut with a knife blade in the center of the transverse grain. Then, the cracks in the cross-section of the veneer in transverse direction were observed via stereo microscope. The pictures were taken by a micro-digital camera and processed into binary images by the iteration threshold method (Bresson et al. 2007). The number of bars and the measurement of fracture depth were processed through ImagePro plus software. The veneer lathe checks rate was calculated according to Eq. 1:

$$\text{Veneer lathe cracks rate}(\%) = \frac{\Sigma L}{n \cdot s} \times 100\% \quad (\%) \tag{1}$$

where: $L$ - the depth of each crack (mm),
$n$ - the number of crack depth less than 50 mm,
$s$ - the thickness of veneer (mm).

### Scanning and records

Five veneers with a size of 400 × 400 mm were taken from each of the three types of veneers. The backside of each veneer was divided into 100 mm meshes, and a special reflective punctuation point (reflective diameter 6 mm) with a diameter of 10 mm was placed at the intersection of meshes. Then, the deformation model of the veneer after air drying could be obtained by scanning in the light strip mode using HandySCAN 700 non-contact 3D laser scanner.

### Image generation and data analysis

VX elements software (VX elements 4.1, Ametek, USA) was used to process the noise of the point cloud, remove isolated islands, and prune the meshes of the model data. The 3D coordinates of grid points and positioning points were processed by the 3D geometric transformation method. A new grid was created by the Cline and Renka scattered data point triangulation method, and overlapping areas were merged to provide uniform point spacing. The meshed "point cloud" allowed the construction of separate 3D images for each veneer.

The 3D coordinates of grids and positioning points were generated by VX elements software, and the space lengths of the veneer along-line direction, cross-line direction, and diagonal direction were calculated (accurate to 0.01 mm). Through the generated contour map, the deflection angle along the grain axis direction was measured, and the maximum deformation height of the veneer was calculated (accurate to 0.01 mm). The warpage degree, D (%), was calculated according to Eq. 2:

$$D(\%) = \frac{h}{L} \times 100\% \quad (\%) \tag{2}$$

where: $h$ - the maximum deformation height of the veneer (mm),
$L$ - the minimum diagonal space length of the veneer (mm).

## RESUTLS AND DISCUSSION

### Lathe checks of veneer

Fig. 1 shows a binary image of the lathe checks of veneer. When the logs of *Taxodium* hybrid 'zhongshanshan' were being cut, the veneer changed from bending state to reverse bending state under the splitting force of the rotary knife.

*Fig. 1: Binary image of lathe checks.*

When the Log-core Veneer Lathe cut the log, the veneer leaves the log and bends backwards. A tensile stress is generated on the back of the veneer. The edge of the blade is at an angle to the fiber direction of the wood, and the tensile strength perpendicular to grain of the wood is generally only 1/10 to 1/40 of the tensile strength parallel to grain (Svitak et al. 2017). When the tensile stress on the back of the veneer exceeds the tensile strength perpendicular to grain of the wood, a crack is formed on the back of the veneer (Lunguleasa et al. 2014). Because the density of *Taxodium* hybrid 'zhongshanshan' wood was low, the material was light and soft, and the transverse tensile strength of the wood was low; therefore, it was easy to produce lathe checks. The observation results of the lathe checks of the *Taxodium* hybrid 'zhongshanshan' veneer are shown in Tab. 1.

*Tab. 1: Lathe checks of Taxodium hybrid 'zhongshanshan' veneer.*

| Type | Sample number | Average number of cracks per cm | Average lathe checks rate (%) | Average crack angle ( ° ) |
|---|---|---|---|---|
| S | 15 | 6 | 49.22 | 23.7 |
| S-H | | 4.6 | 53.69 | 27.5 |
| H | | 8 | 55.85 | 45.3 |

The morphology of the lathe checks of *Taxodium* hybrid 'zhongshanshan' veneer from sapwood to heartwood was gradually rough. Furthermore, with decreasing diameter of rotary-cut logs, the lathe checks rate on the back of veneers increased. The minimum average lathe checks rate of S-type veneers was 49.22%. The lathe checks rate of S-H-type veneers of 53.69% was similar to that of H-type veneers of 55.85%. However, the crack angle of H-type veneers was relatively large. The cracks of S-H-type veneers were usually deeper than those of H-type veneers, and the cracks of H-type veneers were shallow but numerous, and a number of cracks had large openings. Most of the lathe checks of the *Taxodium* hybrid 'zhongshanshan' veneer were oblique in shape.

Changing of lathe checks rate of the S-type and S-H-type veneer shows that the diameter of wood segment decreased and the back angle increased due to the unchanged angle cut by the log-core veneer lathe. The reverse bending angle of the veneer leaving wood segment increased, and the veneer produced large reverse bending deformation, which resulted in an increase of the veneer lathe checks rate with decreasing diameter. As the diameter of wood segment decreased to H-type veneer, the back angle changed toward being too large and the cutting resistance increased, which led to the vibration of the wood segment or tool holder. The rotary knife did not directly cut off the separated wood fibers, which led to cracks during rotary cutting. The wood fibers were directly torn off from the wood segment and then cut off, resulting in large cracks (Guo et al 2010).

## Laser scanning

The HandySCAN 700 testing principle is based on linear structured light method, which is a 3D structure measurement method based on triangulation technology. The characteristic points were formed by projecting a controllable light structure from a structured light projector to the surface of the object to be measured, and the object surface was photographed via camera. Its positioning accuracy, flexibility, and stability met the application requirements of the current industrial field (Bosch et al. 2001).

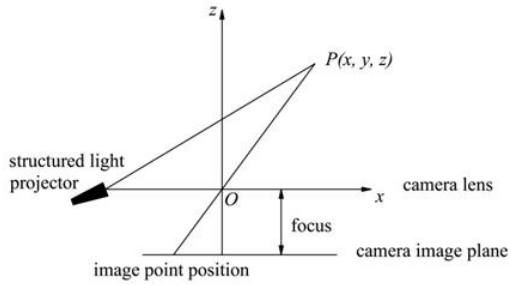


*Fig. 2: Triangle method.*

The principle of triangulation is shown in Fig. 2. The Y-axis of the camera coordinate system O-XYZ was perpendicular to the paper facing inward. It can project light to a point P on the surface of the object to be measured. The projection angle can be obtained by calibrating the external parameters. The position P of the image point can be extracted from the image, and the 3D coordinates of P in the camera coordinate system can be obtained via intersection with the calibration results of the camera parameters.

The scanning mode was light strip, and the basic principle was triangulation. The structured light source used as a linear light source, which moved along the vertical direction of the light strip to scan the back of the veneer. Considering that the center line of the light strip would break when scanning in the light strip mode, which would result in incomplete scanning results (Araki et al. 1995), this study conducted multiple cross-scanning runs on the back of the veneer (Li et al. 2000) to improve the integrity of the scanned data. The maximum glossiness peak of light reflected on the surface of an object occurred when the reflection angle was 60°. The glossiness peaks of marble, stainless steel plate, and flat glass at this angle were larger, and the distribution range was concentrated.

The glossiness distribution of the wood surface was wide and the peak value was low. The glossiness curves in different directions were obviously different. The curves measured under the incidence direction perpendicular to the wood fiber direction were gentler than those measured under the parallel incidence condition. The wood surface was composed of innumerable tiny cells. The reflection on the inner side of the cell wall, after the cell was cut off, formed innumerable tiny concave mirror reflection rays (Li et al. 2018). Due to the anisotropy of wood, the reflection on the inner side of cell wall presented anisotropic reflection, which presented as diffuse reflection on the wood surface or absorbed part of the light (Schaller et al. 2007). In this study, the special reflective punctuation was added when scanning. The depth information of the spot can be obtained because the reflective punctuation had a stronger reflective ability than the wood surface. This can also further improve the scanning accuracy, and provide accurate information for stitching and mesh generation after scanning.

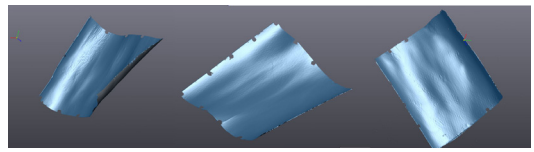

*Fig. 3: Veneer morphology.*

Fig. 3 shows the 3D scanning morphology of deformed veneer after scanning. Using high resolution 3D laser scanning technology not only quantitatively evaluates the deformation of veneer quickly and accurately, but also visually reflects the deformation morphology of veneer. The veneer was rotary cutting when it was green wood, and would then dry naturally below the fiber saturation point. To accurately compare the warpage of veneers, the 3D coordinates of grid points and positioning points were processed with 3D graphic geometric transform method using on the data generated by scanning. The contour map of veneer warpage was reconstructed by using the scattered data points triangulation method by Cline and Renka (Fig. 4, 5, 6).

## Deformation analysis of veneer

Figs. 4, 5, and 6 show that, after air-drying shrinkage, the space length of *Taxodium* hybrid 'zhongshanshan' veneer in transverse dimension was larger than that in parallel grain direction.

This was because wood is an anisotropic material, and the chord drying shrinkage of wood was greater than its radial drying shrinkage, which led to a smaller veneer size in transverse dimension than in parallel grain direction. After air-drying, the veneer inclined 7-12° along the parallel grain axis direction. This was because the arrangement of S2 microfibrils in the cell wall of *Taxodium* hybrid 'zhongshanshan' was at an angle with the wood axis. After air-drying, the veneer inclined in one direction (Yu et al. 2011).

Tab. 2 shows the warpage degree of *Taxodium* hybrid 'zhongshanshan' veneer. With the decrease of the diameter of rotary-cut logs, the warpage degree of *Taxodium* hybrid 'zhongshanshan' veneer increased. The average warpage degrees of S-type, S-H-type, and H-type veneers were 21.18%, 28.20%, and 40.88%, respectively.

*Tab. 2: Warpage degree of Taxodium hybrid 'zhongshanshan' veneer.*

| Veneer type | Sample number | Warpage degree (%) | Average warpage degree (%) |
|---|---|---|---|
| S | S1 | 20.67 | 21.18 |
| | S2 | 23.75 | |
| | S3 | 21.85 | |
| | S4 | 20.68 | |
| | S5 | 18.96 | |
| S-H | S-H1 | 30.83 | 28.20 |
| | S-H2 | 27.04 | |
| | S-H3 | 25.99 | |
| | S-H4 | 29.89 | |
| | S-H5 | 27.28 | |
| H | H1 | 48.67 | 40.88 |
| | H2 | 42.08 | |
| | H3 | 39.21 | |
| | H4 | 36.13 | |
| | H5 | 38.30 | |

The reference planes of Figs. 4, 5, and 6 were diagonally constructed planes of a pair of veneers. The maximum deformation height was the sum of positive and negative extremes of contours. Figs. 4, 5, and 6 show that the maximum deformation height ranking was S-type veneer < S-H-type veneer < H-type veneer.

Wood shrinkage would cause stress and result in deformation. During the air-drying process, the moisture content of the front and back of veneer first decreased below the fiber saturation point, and the front and back of veneer would shrink. Because the moisture content inside the veneer was still above the fiber saturation point, it would be restrained by the inner layer (Goreshnev et al. 2018). At the initial stage of air drying, the area of moisture content on the veneer cross section falling below the fiber saturation point was thinner, the area of tensile stress was smaller, the area of compressive stress was larger, and the total tension and pressure were relatively balanced. Therefore, the tensile stress on the unit area of the front and back of the veneer was very large. When the stress exceeded the limit set by the wood proportion, the veneer would produce plastic deformation. Even though the stress did not exceed the proportional limit, it took a long time to exert force, which resulted in creep and plastic fixation (Muleller et al. 2003).

The lather cracks of *Taxodium* hybrid 'zhongshanshan' veneer caused by rotary cutting are detailed in Tab. 1. The lather cracks led to a larger back surface area than the front surface area, and the stress produced by the back surface was greater than that produced by the front, which resulted in the veneer bending inward from the back. As the diameter of logs decreased during rotary cutting, the lather cracks rate on the back of veneer increased gradually, and the warpage ranking was S-type veneer < S-H-type veneer < H-type veneer.

## Deformation analysis of S-type veneer

Fig. 4 shows a typical deformation of S-type veneer, showing that the whole veneer inclined to the left by 7°. Compared to the reference plane, the highest deformation position was located at the lower right corner of the veneer at +67.24 mm. The lowest deformation position was located at the top boundary of the veneer length direction at -33.66 mm. The maximum difference of the deformation was 100.90 mm, the minimum diagonal space length was 487.87 mm, and the warpage degree was 20.68%. In the central area of the veneer, there were obvious bulges outside this area, and the lather cracks rate of S-type veneer was small. When the gradient of the water content inside and outside veneer tended to be identical, the shrinkage of the surface layer stopped due to plasticization fixation. When the increase of the internal layer resulted from the pre-compressive stress exceeded the proportional limit, compression plasticization fixation occurred with time. Because the compression of the inner layer of veneer was not as large as that of the surface layer of veneer, the shrinkage of the inner layer of veneer was constrained by the hardened surface, and the tensile stress occurred in inner layer and the compressive stress occurred in the surface layer (Ozyhar et al. 2012).

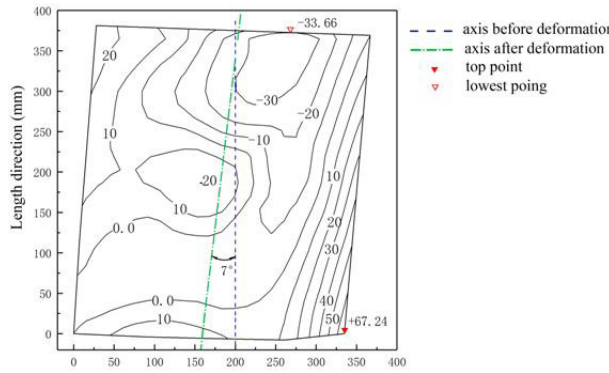


*Fig. 4: Deformation contour map of S type veneer.*

When the tensile stress of the inner layer exceeded the surface compressive stress in specific areas of the veneer, the veneer would deform in the opposite direction of bending, and a bulge would form on the back area of the veneer. From a visual observation of the specimens, the wood texture color at 1/4 of the left side of the width direction of the tested veneer was obviously deeper than that of the right side, and this was the late wood part. The density of the late wood part was higher than that of the early wood, and the corresponding physical and mechanical properties were higher than that of the early wood (Cavalheiro et al. 2018). When the veneer had deformed, it could withstand more surface tension; therefore the warpage deformation of the late wood part of the veneer was smaller than that of the early wood part.

## Deformation analysis of S-H-type veneer

Fig. 5 shows a typical deformation of S-H type veneer, showing that the whole veneer inclined 12° to the left. Compared to the reference plane, the highest deformation position was located at the lower right corner of the veneer at +79.57 mm, the lowest deformation was located at the top boundary of the veneer length direction at -63.70 mm, the maximum difference of deformation was 143.27 mm, the minimum diagonal space length was 525.25 mm, and the warpage degree was 27.28%. The contraction of the veneer in the long space direction was not very different from that of the typical S-type veneer, but in the width space direction, it was larger than that of the typical S-type veneer.

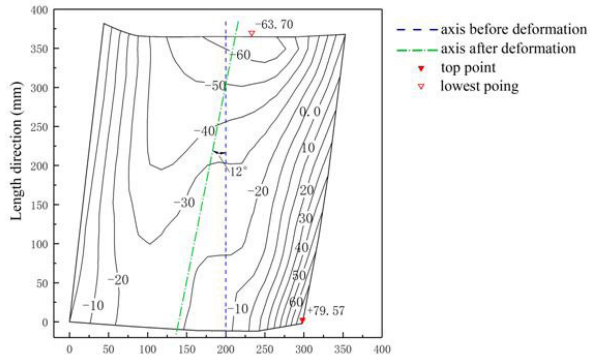


*Fig. 5: Deformation contour map of S-H type veneer.*

The warpage deformation of the right side of the veneer was obviously larger than that of the left side. The warpage deformation was more uniform than that of the typical S-type veneer. Visual observation of the samples showed that the tested veneer was a sapwood part; however, on the left side of the veneer, there were three knots with a diameter of about 15 mm. The knots were formed by living branches of the trees. The wood tissues of the knots were all closely connected to the surrounding wood tissues. When the living knots died, the division of cambium stopped, but the cambium of the main stem continued to divide, and the continuity of the wood tissue between the branches and the main stem was destroyed. As the cambium of the main stem continued to divide, the dead knots were gradually hidden in the xylem of the main stem and formed into hidden knots which were difficult to observe on the outside. Both the wood texture and density around knots differed from that around the wood, which reduced the tensile and compressive of the parallel grain, and flexural strength, but increased the compressive and shear strength of cross striation (Grazide et al. 2018). This inhibited the warpage deformation of the veneer in this part.

## Deformation analysis of H-type veneer

Fig. 6 shows a typical H-type veneer, showing that the whole veneer inclined to the left by 8°. Compared to the reference plane, the highest deformation position was located at the upper left corner of the veneer at +101.35 mm, the lowest deformation position was located at the bottom boundary of the veneer length direction at 93.22 mm, the maximum difference of deformation was 194.57 mm, the minimum diagonal space length was 462.38 mm, and the warpage was 42.08%. The warpage deformation of the left side of the veneer was larger than that of the right side. The warpage deformation of the width direction of H-type veneer was opposite to that of the other two types of veneers. Visual observation of the specimens indicated that there was a large number of knots in the middle of the width direction of the veneer from bottom to the top 3/4,

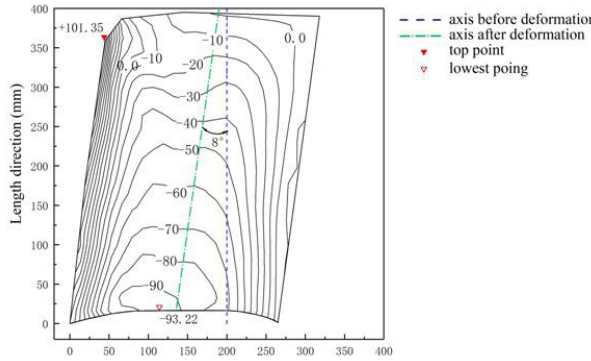


*Fig. 6: Deformation contour map of H type veneer.*

and the knots gradually decreased in size and number from bottom to top. The knots affected the deformation of the lower half of the veneer, enlarging the deformation of other areas.

The above analysis shows that the veneer warped mainly in the width direction, which was mainly because the tensile strength along parallel to the grain of wood was generally the maximum strength of the wood; therefore, the veneer did not warp in the length direction. The transverse tensile strength of the wood was typically very low, which resulted in a large warpage of veneer in width direction. In the veneer, there were wood material differences between heartwood and sapwood, as well as between early wood and late wood. The knots and lather crack size in the process of rotary cutting were also different. Therefore, the moisture content did not uniformly decrease during air drying, which led to different time of each part to air drying state, and then further led to the difference of veneer warpage.

## CONLUSIONS

High-resolution 3D laser scanning technology can intuitively and quickly measure veneer deformation. Increasing reflective markers can increase the accuracy of measurement. Veneer warpage was affected by the size of lather cracks, and the larger the lather cracks, the greater the veneer warpage. Veneer warpage deformation was related to the transverse tensile strength of wood. The warpage of each part of the veneer differed, because veneer is a heterogeneous material with anisotropy.

After air-drying shrinkage of *Taxodium* hybrid 'zhongshanshan' veneer, the space length in transverse direction was clearly larger than that in parallel grain direction, and after air-drying, the veneer would deflect along the direction of the parallel axis. With decreasing diameter of rotary cutting logs, the warpage of the *Taxodium* hybrid 'zhongshanshan' veneer increased. The average warpage degree in the sapwood part was 21.18% with 7° of deflection, that of intermediate wood part 28.20% with 12° of deflection, and that of heartwood near piths 40.88% with 8° of deflection.

## ACKNOWLEDGMENT

This research was supported by the Jiang Su agricultural science and technology innovation fund (grant no. CX(16)1005) and by the Plant germplasm resources innovation project of

Strategic bioresources service network of Chinese Academy of Sciences (grant no. ZSZC-009). The received financial support is gratefully acknowledged.

## REFERENCES

1. Araki, K., Shimizu, M., Noda, T., Chiba, Y., Tsuda, Y., Ikegaya, K., Sannomiya, K., Gomi, M., 1995: A high-speed and continuous 3d measurement system. Machine Vision and Applications 8(2): 79-84.
2. Bartosz, P., Rémy, M., Butaud, J.C., Denaud, L.E., Kowaluk, G., 2010: A method of lathe checks measurement; SMOF device and its software. European Journal of Wood and Wood Products 68(2): 151-159.
3. Bosch, T., Lescure, M., Myllyla, R., Rioux, M., Amann, M.C., 2001: Laser ranging: a critical review of usual techniques for distance measurement. Optical Engineering 40(1): 10-19.
4. Bresson, X., Esedog, L.S., Vandergheynst, P., Thiran, J.P., Osher, S., 2007: Fast global minimization of the active contour/snake model. Journal of Mathematical Imaging and Vision 28(2): 151-167.
5. Cavalheiro, R., Almeida, D., Almeida, T., André, C., Lahr, F., 2018: Estimation of modulus of elasticity in static bending of wood in structural dimensions as a function of longitudinal vibration and density. Current Journal of Applied Science & Technology: 26(1): 1-8.
6. Goreshnev, M.A., Sekisov, F.G., Smerdov, O.V., 2018: Determination of the coefficient of thermal and moisture conductivity of wood by the transient moisture current method. Journal of Engineering Physics & Thermophysics 91(3): 827-830.
7. Grazide, C., Coureau, J.L., Cointe, A., Morel, S., 2018: Mechanical performance curves for the strength grading of Maritime pine. European Journal of Wood & Wood Product 76(3): 877-888.
8. Gui, R., Xu, X., Zhang, D.J., Lin, H., Pu, F.L., He, L., Cao, M., 2018: A component decomposition model for 3d laser scanning pavement data based on high-pass filtering and sparse analysis. Sensors 18(7): 2294.
9. Guo, Y.H., Li Y.H., Yang, L.M., 2010: Feed rate servo control for spindle-less veneer lathe. Proceeding of 4th International Conference on Robotics, Automation and Mechatronics. Singapore: IEEE: Pp 315-320.
10. Hua, J.F., Han, L.W., Gu, C.S., Yin, Y.L., 2017: Morpho-anatomical and photosynthetic responses of *Taxodium* hybrid 'Zhongshanshan' 406 to prolonged flooding. Flora 231(6): 29-37.
11. Lunguleasa, A., Coseseanu, C., Budau, G., Lica, D., Matei, MG., 2014: Contributions to the curvature radius and bending capacity of veneers. Wood Research 59(5): 843-850.
12. Kong, F.X., Song, T.Y., Chai, H.J., Cai, Y.C., 2018: Radio-frequency vacuum drying for oak veneer. Journal of Northeast Forestry University 46(6): 81-88 (in Chinese).
13. Krajewski, G., Woz'niak, A., 2014: Simple master artefact for CMM dynamic error identification. Precision Engineering 38 (1): 64-70.
14. Li, Q., Griffiths, J.G., 2000: Iterative closest geometric objects registration. Computers and Mathematics with Applications 40(10): 1171-1188.
15. Li, T., Liu, H., Zhao, X.P., Chen, G., Dai, J.Q., Pastel, G., Jia, C., Chen C.J., Hitz, E., Das, S., Yang, R.G., Hu, L.B., 2018: Scalable and highly efficient mesoporous wood-based solar steam generation device: Localized heat, rapid water transport. Advanced Functional Materials 28(16): 1707134.

16. Lobb, M., Krawiec, K., Howard, A.J., Gearey, B.R., Chapman, H.P., 2010: A new approach to recording and monitoring wet-preserved archaeological wood using 3D laser scanning. Journal of Archaeological Science 37(12): 2995-2999.
17. Mbarek, T.B., Robert, L., Hugot, F., Orteu, J.J., 2011: Mechanical behavior of wood-plastic composites investigated by 3d digital image correlation. Journal of Composite Materials 45(26): 2751-2764.
18. Müller, U., Gindl, W., Teischinger, W., 2003: A. Effects of cell anatomy on the plastic and elastic behaviour of different wood species loaded perpendicular to grain. IAWA Journal 24(2): 117-128.
19. Olenska, S., Margraf, T., Beer, P., 2014: An analysis of a method of Asymmetrical veneering for furniture element, veneered with bamboo mats. Bioresources 9(1): 566-577.
20. Ozyhar, T., Hering, S., Niemz, P., 2012: Moisture-dependent elastic and strength anisotropy of european beech wood in tension. Journal of Material Science 47(16): 6141-6150.
21. Rafał, K., Michał, R., Łukasz, O., 2018: Measurement point density and measurement methods in determining the geometric imperfections of shell surfaces. Reports on Geodesy and Geoinformatics 105: 19-28.
22. Schaller, C., Rogez, D., 2007: New approaches in wood coating stabilization. Journal of Coatings Technology & Research 4(4): 401-409.
23. Scott, C.T., Hernandez, R., Frihart, C., Gleisner, R., Tice, T., 2005: Method for quantifying percentage wood failure in block-shear specimens by a laser scanning profilometer. Journal of ASTM International 2(8): 1-10.
24. Shi, Q., Yin, Y.L., Wang, Z.Q., Fan, W. C., Hua, J.F., 2016: Physiological acclimation of *Taxodium* hybrid 'zhongshanshan 118' plants to short-term drought stress and recovery. Hort Science 51(9): 1159–1166.
25. Svitak, M., Ruman, D., 2017: Tensile-shear strength of layerd wood reinforced by carbon materials. Wood Research 62(2): 243-251.
26. Wang, J., Biernacki, J.M., Lam, F., 2001: Nonderstructive evaluation of veneer quality using acoustic wave measurements. Wood Science and Technology 34: 505-516.
27. Yu, H.Q., Fei, B.H., Zhao, R.J., Liu, J.L., Zhang, X.Y., 2007: Anatomical Characteristics of *Taxodium* 'zhongshansa302' and *Taxodium* distichum Wood. Forest Research 20(2): 213-217 (in Chinese).
28. Yu, Y., Fei, B.H., Wang, H.K., Tian, G.L., 2011: Longitudinal mechanical properties of cell wall of Masson pine (*Pinus massoniana* Lamb.) as related to moisture content: A nanoindentation study. Holzforschung 65(1): 121-126.
29. Zhao, R.J., Fei, B.H., Yu, H.Q., Liu, J.L., 2007: Physical and mechanical properties of *Taxodium* 'zhongshansha 302' and *Taxodium* distichum wood. Journal of Northeast Forestry University 35(2): 4-6 (in Chinese).

Zhu Yuehua*, Pan Biao, Zhang Yaoli
Nanjing Forestry University
College of Materials Science and Engineering
Nanjing 210037
China
*Corresponding author: otakuzhu@outlook.com